Available online at www.sciencedirect.com

ScienceDirect

IFAC Papers Online CONFERENCE PAPER ARCHIVE

IFAC PapersOnLine 58-28 (2024) 438–443

Maneuvering an Autonomous Spatial Unicycle

Máté B. Vizi [*,**] **Gábor Orosz** [***,****] **Dénes Takács** [*,**] **Gábor Stépán** [*,**]

[*] *Department of Applied Mechanics, Budapest University of Technology and Economics, Budapest, Hungary (e-mails: {vizi,takacs,stepan}@mm.bme.hu)*

[**] *HUN-REN–BME Dynamics of Machines Research Group, Budapest, Hungary*

[***] *Department of Mechanical Engineering, University of Michigan, Ann Arbor, MI 48109, USA (e-mail: orosz@umich.edu)*

[****] *Department of Civil and Environmental Engineering, University of Michigan, Ann Arbor, MI 48109, USA*

Abstract: The path-following task of an autonomous unicycle is considered in the three-dimensional space. The equation of motion is derived using the Appellian aproach of non-honolomic dynamics. The resulting nonlinear model is transformed into the path-reference frame. Using pole placement, a linear feedback controller is designed that takes into account the velocity of the maneuver. The resulting controller is tested on the nonlinear model via numerical simulations; lane change maneuvers are carried out successfully at different speeds.

Keywords: Path Planning and Motion Control; Control Design; Robotics

1. INTRODUCTION

Micromobility devices such as electric unicycles and scooters are rapidly spreading in urban environments as their compact size is paired with agility and maneuverability. These properties are so attractive that researchers started develop and build various types of autonomous unicycles. Common approaches used inverted pendulums (Zenkov et al., 2002), flywheels (Vos and von Flotow, 1990; Geist et al., 2022; Cao et al., 2023), gyroscopes (Brown and Xu, 1996) or the combination of those (Schoonwinkel, 1987) for controlling the unicycles. Suzuki et al. (2014) even developed a humanoid-type autonomous unicycle while the Ringbot (Gim and Kim, 2024) used two robotic arms for control. Yet, the motion planning and control design of the underlying nonlinear dynamical systems is barely understood.

It is challenging to find a simplistic, yet high-fidelity modeling framework, which enables one to describe the spatial dynamics of the unicycle, including the yaw, tilt, and pitch motions, see Fig. 1. While multi-body softwares can be used, they produce complex models which are not applicable for control design. The kinematic constraints for rolling shall be incorporated while the use of Lagrange multipliers is not desired as those lead to differential

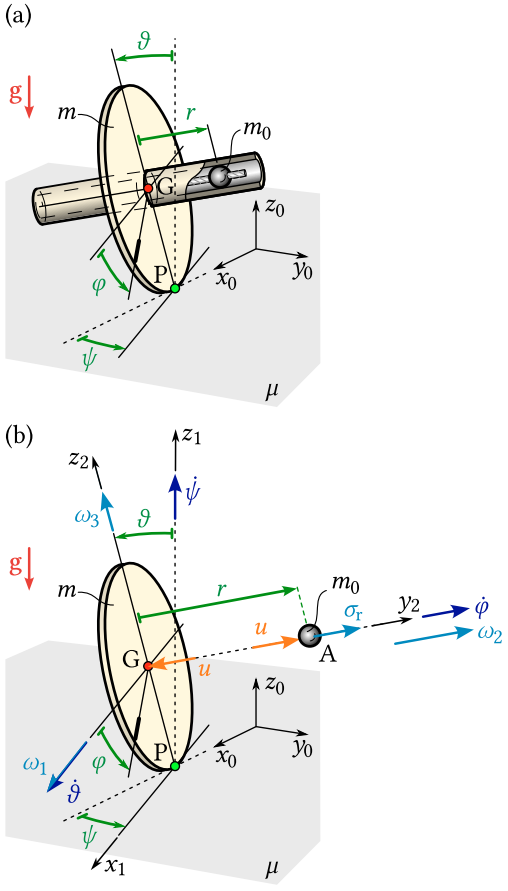

Fig. 1. Unicycle model (a), kinematic quantities (b)

⋆ This research was partly supported by the National Research, Development and Innovation Office of Hungary under grants NKFI-146201, NKFI-KKP-133846 and by the HUN-REN Hungarian Research Network. DT is supported by the János Bolyai Research Scholarship of the Hungarian Academy of Sciences. GO acknowledges the support of the Hungarian Academy of Sciences within the Distinguished Guest Fellowship Programme and the support of the Fulbright Foundation.

10.1016/j.ifacol.2025.01.085

algebraic equations which again make control design very challenging. The designed controllers shall be applicable to the nonlinear system without large computational burden.

In this work we build on our previous modeling efforts about the spatial dynamics of an autonomous unicycle (Vizi et al., 2023) and focus on maneuvering the unicycle while following a planned path. We control the lateral motion by means of shifting the center of gravity via moving a point mass with a single actuator, see Fig. 1. The dynamics of this nonholonomic system are derived by using the Appellian approach, which takes into account the rolling constraints. In this work, the path-following problem is investigated such that the equations of motion are transformed from the original Earth fixed coordinates to a moving path-following reference frame. This way, the lateral error and the alignment error can directly be utilized in the control law. Taking into account the velocity of the unicycle, a linear feedback controller is designed to follow the path. The control performance is verified via numerical simulations of the nonlinear equations.

2. GOVERNING EQUATIONS

The unicycle is modeled as a disc with mass m and radius R that rolls on the horizontal ground, see Fig. 1. The point mass m_0 can be moved along the wheel axle by the internal force u which is the control input. The gravitational acceleration is denoted by g.

Without any constraints, the autonomous unicycle that consists of one rigid body and one point mass, has $N = 6 + 3 = 9$ degrees of freedom. The position of the wheel is described by

$$\mathbf{r}_{\mathrm{G}} = [x_{\mathrm{G}} \quad y_{\mathrm{G}} \quad z_{\mathrm{G}}]^{\mathsf{T}}_{\mathrm{F}_0} \tag{1}$$

of the disc center G for which the vector components $x_{\mathrm{G}}, y_{\mathrm{G}}$ and z_{G} are resolved in the earth-fixed frame F_0. The orientation of the disc is given by the yaw, tilt and pitch angles, ψ, ϑ and φ, respectively. The position of the mass at point A, relative to the wheel center G, is given by the three coordinates of the vector $\mathbf{r}_{\mathrm{GA}}$.

The wheel is assumed to be rolling without slipping; for the three-dimensional rolling and slipping transition please see (Antali and Stépán, 2019). The kinematic condition for rolling is that the point P of the wheel instantaneously contacting the ground is the velocity pole point for which

$$\mathbf{v}_{\mathrm{P}} = \mathbf{0}, \tag{2}$$

holds. Also, the velocity $\mathbf{v}_{\mathrm{P}}$ can be expressed via the transport formula

$$\mathbf{v}_{\mathrm{P}} = \mathbf{v}_{\mathrm{G}} + \boldsymbol{\omega} \times \mathbf{r}_{\mathrm{GP}}. \tag{3}$$

Here $\mathbf{v}_{\mathrm{G}}$ is the velocity of the center of gravity G which can be resolved in the ground-fixed frame F_0 as

$$\mathbf{v}_{\mathrm{G}} = \dot{\mathbf{r}}_{\mathrm{G}} = [\dot{x}_{\mathrm{G}} \quad \dot{y}_{\mathrm{G}} \quad \dot{z}_{\mathrm{G}}]^{\mathsf{T}}_{\mathrm{F}_0}, \tag{4}$$

while the angular velocity $\boldsymbol{\omega}$ of the wheel and the relative position $\mathbf{r}_{\mathrm{GP}}$ of the contact point P with respect to the wheel center G is given in the moving frame F_2 as

$$\begin{aligned} \boldsymbol{\omega} &= \big[\dot{\vartheta} \quad \dot{\varphi} + \dot{\psi}\sin\vartheta \quad \dot{\psi}\cos\vartheta\big]^{\mathsf{T}}_{\mathrm{F}_2}, \\ \mathbf{r}_{\mathrm{GP}} &= [0 \quad 0 \quad -R]^{\mathsf{T}}_{\mathrm{F}_2}. \end{aligned} \tag{5}$$

The kinematic condition (2) of rolling together with (3)–(5) yield $n_{\mathrm{k}} = 2$ kinematic constraints

$$\begin{aligned} \dot{x}_{\mathrm{G}} &= \omega_1 R\sin\psi\cos\vartheta + \omega_2 R\cos\psi, \\ \dot{y}_{\mathrm{G}} &= -\omega_1 R\cos\psi\cos\vartheta + \omega_2 R\sin\psi, \end{aligned} \tag{6}$$

and one geometric constraint

$$\dot{z}_{\mathrm{G}} = -\dot{\vartheta}R\sin\vartheta \quad \Rightarrow \quad z_{\mathrm{G}} = R\cos\vartheta. \tag{7}$$

Also, the point mass at point A is allowed to move along the wheel axle which can be formulated as

$$\mathbf{r}_{\mathrm{GA}} = [0 \quad r \quad 0]^{\mathsf{T}}_{\mathrm{F}_2}, \tag{8}$$

yielding two more geometric constraints, so the system has $n_{\mathrm{g}} = 3$ geometric constraints in total.

We opt for using the Appellian approach (Appell, 1900) to derive the equations of motion of the unicycle. This pseudo velocity based method directly yields a system of first order ordinary differential equations, which is the most compact representation of the underlying nonholonomic mechanical system. Moreover, the appropriate definition of the pseudovelocities significantly reduces the algebraic complexity of the equations of motion which further ease the dynamical analysis and the control design. These benefits render the Appellian approach superior to the well-known generalized Lagrangian equations in this example.

To describe the system with the minimal number of coordinates after considering the geometric constraints, one must intuitively choose $n_q = N - n_{\mathrm{g}} = 6$ generalized coordinates that unambiguously describe the spatial configuration of the system. We describe the position of the unicycle with the wheel center positions x_{G} and y_{G}, while the orientation is given by the angles ψ, ϑ, φ. Note that the vertical position z_{G} can be obtained using the geometric constraint (7). The relative position r determines the location of the point mass; to sum up, the generalized coordinates are

$$x_{\mathrm{G}},\ y_{\mathrm{G}},\ \psi,\ \vartheta,\ \varphi,\ r. \tag{9}$$

Similarly, due to the pure rolling and the related kinemaic constraints one should define $n_\sigma = 9 - n_{\mathrm{g}} - n_{\mathrm{k}} = 4$ pseudo velocities which are defined as the components of the angular velocity $\boldsymbol{\omega}$, resolved in frame F_2 in (5), and the velocity component of m_0 parallel to the wheel axle:

$$\begin{aligned} \omega_1 &:= \dot{\vartheta}, & \omega_2 &:= \dot{\varphi} + \dot{\psi}\sin\vartheta, \\ \omega_3 &:= \dot{\psi}\cos\vartheta, & \sigma_{\mathrm{r}} &:= \dot{r} - \dot{\vartheta}R. \end{aligned} \tag{10}$$

The kinematics of the systems is described by (6) and (10) while the remaining four dynamical equations can be derived using the Appellian approach as in (Vizi et al., 2023). Following this method, the equations of motion become

$$\begin{aligned} \dot{\omega}_1 &= \frac{1}{5mR^2 + 4m_0r^2}\big(-4\omega_1^2 m_0 Rr - 8\omega_1\sigma_{\mathrm{r}} m_0 r \\ &\quad - \omega_3^2(mR^2\tan\vartheta + 4m_0r^2\tan\vartheta) + 4mgR\sin\vartheta \\ &\quad + \omega_2\omega_3(6mR^2 + 4m_0Rr\tan\vartheta) - 4m_0gr\cos\vartheta \\ &\quad + 4Ru\big), \\ \dot{\omega}_2 &= \frac{2}{3mR^2 + 2m_0R^2 + 12m_0r^2}\big(-2\omega_1\omega_2 m_0 Rr \\ &\quad + \omega_1\omega_3(m_0R^2 - mR^2 - 4m_0r^2) + 2\omega_3\sigma_{\mathrm{r}} m_0 R\big), \\ \dot{\omega}_3 &= \frac{1}{3mR^2 + 2m_0R^2 + 12m_0r^2}\big(-24\omega_3\sigma_{\mathrm{r}} m_0 r \\ &\quad - \omega_1\omega_2(6mR^2 + 4m_0R^2) + \omega_1\omega_3\big((3mR^2 \\ &\quad + 2m_0R^2 + 12m_0r^2)\tan\vartheta - 20m_0Rr\big)\big), \end{aligned} \tag{11}$$

$$
\begin{aligned}
\dot{\sigma}_\mathrm{r} &= \omega_1^2 r + \omega_3^2 r - \omega_2\omega_3 R - g\sin\vartheta + \frac{1}{m_0}u,\\
\dot{\vartheta} &= \omega_1,\\
\dot{r} &= \omega_1 R + \sigma_\mathrm{r},\\
\dot{\psi} &= \omega_3 \frac{1}{\cos\vartheta},\\
\dot{\varphi} &= \omega_2 - \omega_3\tan\vartheta,\\
\dot{x}_\mathrm{G} &= \omega_1 R\sin\psi\cos\vartheta + \omega_2 R\cos\psi,\\
\dot{y}_\mathrm{G} &= -\omega_1 R\cos\psi\cos\vartheta + \omega_2 R\sin\psi.
\end{aligned}
\tag{11}
$$

3. PATH-FOLLOWING PROBLEM

In case of a path-following task, it is beneficial to define the problem relative to the desired path such as shown in Fig. 2. We consider to follow the desired path with the geometric wheel-ground contact point.

In each time instant, a different material point P of the wheel contacts the ground as the wheel rolls forward. This material point P is also called velocity pole since $\mathbf{v}_\mathrm{P} = \mathbf{0}$, cf. (2). The point P also frequently called as the instantaneous center of velocities or the instantaneous center of rotation. The circumferential points of the wheel are called the moving polode. On the other hand, the wheel-ground contact point is a geometric point denoted by P′ moving on the surface of the ground as the wheel rolls forward. The trace of P′ can be thought of as a curvilinear path painted on the ground by the rolling wheel. The path of the geometric pole P′ is called the fixed polode. During rolling, the material point P becomes steady for a single time instance, $\mathbf{v}_\mathrm{P} = \mathbf{0}$, cf. (2), while the the geometric pole P′ is moving along the fixed polode with velocity $\mathbf{v}_{\mathrm{P}'} \neq \mathbf{0}$.

The position of the geometric pole can be calculated by

$$
\mathbf{r}_{\mathrm{P}'} = \mathbf{r}_\mathrm{G} + \mathbf{r}_{\mathrm{GP}'} = [x_{\mathrm{P}'} \quad y_{\mathrm{P}'} \quad 0]^\mathsf{T}_{\mathrm{F}_0}, \tag{12}
$$

where $\mathbf{r}_{\mathrm{GP}'} = \mathbf{r}_\mathrm{GP}$ holds instantaneously. Using (1), (6) and (12), the pole changing velocity can be obtained as

$$
\mathbf{v}_{\mathrm{P}'} = \dot{\mathbf{r}}_{\mathrm{P}'} = [\dot{x}_{\mathrm{P}'} \quad \dot{y}_{\mathrm{P}'} \quad 0]^\mathsf{T}_{\mathrm{F}_0}, \tag{13}
$$

where

$$
\begin{aligned}
\dot{x}_{\mathrm{P}'} &= \omega_2 R\cos\psi - \omega_3 R\tan\vartheta\cos\psi,\\
\dot{y}_{\mathrm{P}'} &= \omega_2 R\sin\psi - \omega_3 R\tan\vartheta\sin\psi.
\end{aligned}
\tag{14}
$$

A more detailed discussion about the velocity pole and the pole changing velocity in case of three dimensional spatial motions can be found in Csernák (2019).

Instead of the wheel center position $(x_\mathrm{G}, y_\mathrm{G})$, the velocity pole position $(x_{\mathrm{P}'}, y_{\mathrm{P}'})$ can be used as system states conforming to the path-following goal. Similarly, the kinematic constraints (6) can be replaced by the pole changing velocity (14) in the last two equations of the dynamical model (11).

In (Qin et al., 2022), a general method is developed to transform the original absolute position and orientation (x, y, ψ) to a moving reference frame (ξ, η, θ) attached to the desired path. Also, by finding the point of the desired path closest to P′, see point D in Fig. 2, one can express the current position using the arc length s along the desired path and the lateral deviation ε from the path, while the orientation can be given by the relative yaw angle θ. The evolution of the variables s, ε and θ can be given as

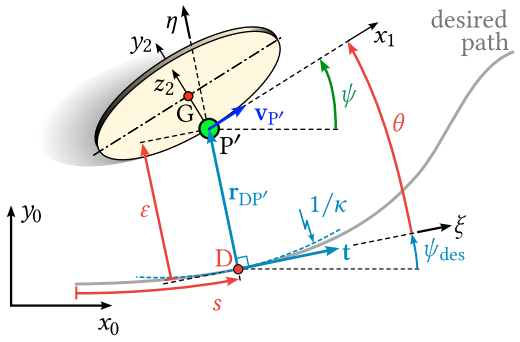

Fig. 2. Coordinate transformation for path following

$$
\begin{aligned}
\dot{s} &= \frac{1}{1-\kappa\varepsilon}\left(\dot{x}_{\mathrm{P}'}\cos\psi_\mathrm{des} + \dot{y}_{\mathrm{P}'}\sin\psi_\mathrm{des}\right),\\
\dot{\varepsilon} &= -\dot{x}_{\mathrm{P}'}\sin\psi_\mathrm{des} + \dot{y}_{\mathrm{P}'}\cos\psi_\mathrm{des},\\
\dot{\theta} &= \dot{\psi} - \frac{\kappa}{1-\kappa\varepsilon}\left(\dot{x}_{\mathrm{P}'}\cos\psi_\mathrm{des} + \dot{y}_{\mathrm{P}'}\sin\psi_\mathrm{des}\right),
\end{aligned}
\tag{15}
$$

where $\psi_\mathrm{des}(s)$ is the desired yaw angle and $\kappa(s) = \frac{\mathrm{d}\psi_\mathrm{des}}{\mathrm{d}s}(s)$ $[\mathrm{m}^{-1}]$ is the *signed* curvature at the same point, for which $\kappa > 0$ means a left turn, while $\kappa < 0$ is a right turn.

The geometric pole P′ is chosen as the reference point for path-following. Therefore, one can substitute the corresponding pole changing velocity components $\dot{x}_{\mathrm{P}'}$ and $\dot{y}_{\mathrm{P}'}$ into the transformation (15) through the kinematic constraints (14) to obtain

$$
\begin{aligned}
\dot{s} &= \frac{1}{1-\kappa\varepsilon}\left(\omega_2 R\cos\theta - \omega_3 R\cos\theta\tan\vartheta\right),\\
\dot{\varepsilon} &= \omega_2 R\sin\theta - \omega_3 R\sin\theta\tan\vartheta,\\
\dot{\theta} &= \frac{-1}{(1-\kappa\varepsilon)\cos\vartheta}\big(\omega_2 R\kappa\cos\theta\cos\vartheta\\
&\qquad - \omega_3\left(1 - \kappa\varepsilon + R\kappa\sin\vartheta\cos\theta\right)\big).
\end{aligned}
\tag{16}
$$

where $\theta = \psi - \psi_\mathrm{des}$. For control design, the equations related to the original states $(x_{\mathrm{P}'}, y_{\mathrm{P}'}, \psi)$ in the dynamical model (11) can be replaced by the path-related states s, ε, θ using (16).

The desired path can be given by the curvature $\kappa(s)$ as the function of the arc length s. In this study, a lane change parallel to the x axis is chosen to be the desired maneuver. The maneuver start and end with straight sections. The middle part, i.e., the actual lane change, is divided into 3 clothoid segments (Oh et al., 2023) such that the curvature $\kappa(s)$ is a continuous function of the arclenght s along the desired path. Since clothoid segments are used, the curvature $\kappa(s)$ changes linearly with respect to the arc length s during the segments. The desired paths are shown in the bottom panels of Fig. 3 as dashed-dotted black curves.

4. CONTROL DESIGN AND SIMULATIONS

A linear state feedback controller is designed to carry out maneuvers with the autonomous unicycle. We assume that the unicycle has a non-zero initial pitch rate $|\dot{\varphi}_*| > 0$. Furthermore, we consider only maneuvers which require sufficiently small yaw rates $\dot{\psi}$ and tilt angles ϑ. With these assumptions, we use the straight rolling steady state as the basis for control design.

The linearized equations of motion are obtained in the form:

$$\begin{aligned}
\dot{\omega}_1 &= \frac{6}{5}\omega_3\dot{\varphi}_* + \frac{4g}{5R}\vartheta - \frac{4m_0g}{5mR^2}r + \frac{4}{5mR}u,\\
\dot{\hat{\omega}}_2 &= 0,\\
\dot{\omega}_3 &= -2\omega_1\dot{\varphi}_*,\\
\dot{\sigma}_\mathrm{r} &= -\omega_3\dot{\varphi}_*R - g\vartheta + \frac{1}{m_0}u,\\
\dot{\vartheta} &= \omega_1,\\
\dot{r} &= \omega_1 R + \sigma_\mathrm{r},\\
\dot{\varphi} &= \hat{\omega}_2 + \dot{\varphi}_*,\\
\dot{s} &= \hat{\omega}_2 R + \dot{\varphi}_* R,\\
\dot{\varepsilon} &= \dot{\varphi}_* R\theta,\\
\dot{\theta} &= \omega_3,
\end{aligned} \tag{17}$$

by assuming a straight rolling steady state with the pitch rate $\dot{\varphi}_*$ in the arbitrary direction ψ_*. This straight line is considered to be the desired path, that is, so $\psi_\mathrm{des}(s) \equiv \psi_*$ and $\kappa(s) \equiv 0$ is used for control design.

As one may expect, the linearized equations of motion (17) is independent of the direction ψ_*. However, the linearized dynamics strongly depend on the steady state pitch rate $\dot{\varphi}_*$, that must be taken into account in control design. It was shown in (Vizi et al., 2023), in case of the uncontrolled unicycle, that the stability of straight rolling depends on the steady state pitch rate $\dot{\varphi}_*$. Slow unicycles with $|\dot{\varphi}_*| < \dot{\varphi}_\mathrm{crit}$ are unstable, while the fast ones with $|\dot{\varphi}_*| > \dot{\varphi}_\mathrm{crit}$ are (neutrally) stable, where the critical pitch rate is

$$\dot{\varphi}_\mathrm{crit} = \sqrt{\frac{g}{2R}}. \tag{18}$$

The linearized equations (17) correspond to the state space model $\dot{\mathbf{x}} = \mathbf{A}\mathbf{x} + \mathbf{B}u$ with states

$$\mathbf{x} = [\omega_1 \quad \hat{\omega}_2 \quad \omega_3 \quad \sigma_\mathrm{r} \quad \vartheta \quad r \quad \varphi \quad s \quad \varepsilon \quad \theta]^\mathsf{T}, \tag{19}$$

while the system and input matrices become

$$\mathbf{A} = \begin{bmatrix}
0 & 0 & A_{1,3} & 0 & A_{1,5} & A_{1,6} & 0 & 0 & 0 & 0\\
0 & 0 & 0 & 0 & 0 & 0 & 0 & 0 & 0 & 0\\
A_{3,1} & 0 & 0 & 0 & 0 & 0 & 0 & 0 & 0 & 0\\
0 & 0 & A_{4,3} & 0 & A_{4,5} & 0 & 0 & 0 & 0 & 0\\
1 & 0 & 0 & 0 & 0 & 0 & 0 & 0 & 0 & 0\\
R & 0 & 0 & 1 & 0 & 0 & 0 & 0 & 0 & 0\\
0 & 1 & 0 & 0 & 0 & 0 & 0 & 0 & 0 & 0\\
0 & R & 0 & 0 & 0 & 0 & 0 & 0 & 0 & 0\\
0 & 0 & 0 & 0 & 0 & 0 & 0 & 0 & 0 & A_{9,10}\\
0 & 0 & 1 & 0 & 0 & 0 & 0 & 0 & 0 & 0
\end{bmatrix},$$

$$\mathbf{B} = \left[\tfrac{4}{5mR} \quad 0 \quad 0 \quad \tfrac{1}{m_0} \quad 0 \quad 0 \quad 0 \quad 0 \quad 0 \quad 0\right]^\mathsf{T}, \tag{20}$$

with

$$\begin{aligned}
A_{1,3} &= \frac{6}{5}\dot{\varphi}_*, \qquad A_{1,5} = \frac{4g}{5R}, \qquad A_{1,6} = -\frac{4m_0g}{5mR^2},\\
A_{3,1} &= -2\dot{\varphi}_*, \quad A_{4,3} = -R\dot{\varphi}_*, \quad A_{4,5} = -g,\\
&\qquad A_{9,10} = R\dot{\varphi}_*.
\end{aligned} \tag{21}$$

By engineering intuition, the outputs

$$\mathbf{y} = \mathbf{C}\mathbf{x} := [\omega_1 \quad \sigma_\mathrm{r} \quad \vartheta \quad r \quad \varepsilon \quad \theta]^\mathsf{T}, \tag{22}$$

are chosen (with an appropriate output matrix $\mathbf{C}$) to be the states that are relevant for path-following. The state ω_3 which is related to the yaw rate ($\dot{\psi}$ or $\dot{\theta}$) is not included here because it is linearly proportional to the tilt angle ϑ; further details can be found in Vizi et al. (2023).

It can be shown that the linear system (17) cosidering the control outputs (22) is output controllable with the single control input u as the output controllability matrix $\mathbf{M}_\mathrm{oc} = \begin{bmatrix}\mathbf{CB} & \mathbf{CAB} & \dots & \mathbf{CA}^5\mathbf{B}\end{bmatrix}$ has full rank, i.e., $\operatorname{rank}\mathbf{M}_\mathrm{oc} = 6$.

In order to control the unicycle and carry out maneuvers, we apply the linear feedback

$$u := -\mathbf{K}(\mathbf{y} - \mathbf{y}_\mathrm{des}) \tag{23}$$

with the control gains

$$\mathbf{K} = [D_\vartheta \quad D_r \quad P_\vartheta \quad P_r \quad P_\varepsilon \quad P_\theta], \tag{24}$$

and the desired output $\mathbf{y}_\mathrm{des} \equiv \mathbf{0}$.

The characteristic roots $\lambda_i, i = 1, \dots, 6$ of the closed-loop system

$$\det\big(\lambda\mathbf{I} - (\mathbf{A} - \mathbf{BKC})\big) = 0 \tag{25}$$

can be assigned by choosing the control gains as

$$\begin{aligned}
D_\vartheta &= \frac{5mR}{4mg^2 + 48\dot{\varphi}_*^2mgR + 32\dot{\varphi}_*^2m_0gR}\big(5mR^2\Lambda_5\\
&\quad + 5mgR\Lambda_3 + \Lambda_1(4mg^2 - 12\dot{\varphi}_*^2mgR - 8\dot{\varphi}_*^2m_0gR)\big),\\
D_r &= -\frac{5mm_0\left(R^2\Lambda_5 + gR\Lambda_3 + g^2\Lambda_1\right)}{mg^2 + 12\dot{\varphi}_*^2mgR + 8\dot{\varphi}_*^2m_0gR},\\
P_\vartheta &= -\frac{m}{4mg^2 + 48\dot{\varphi}_*^2mgR + 32\dot{\varphi}_*^2m_0gR}\big(\Lambda_6(25mR^3\\
&\quad + 20R^3m_0) + \Lambda_4(25mgR^2 + 20m_0gR^2)\\
&\quad + 20\Lambda_2((m+m_0)g^2R - \dot{\varphi}_*^2(3m - 2m_0)g^2R)\\
&\quad - 48\dot{\varphi}_*^4(3m + 2m_0)gR^2 - 24\dot{\varphi}_*^2(4m - 3m_0)g^2R\\
&\quad + (16m + 20m_0)g^3\big),\\
P_r &= \frac{m_0}{mg^2R + 12\dot{\varphi}_*^2mgR^2 + 8\dot{\varphi}_*^2m_0gR^2}\big(5mR^3\Lambda_6\\
&\quad + 5mgR^2\Lambda_4 + 5mg^2R\Lambda_2 + 4mg^3 - 12\dot{\varphi}_*^2mg^2R\\
&\quad - 8\dot{\varphi}_*^2m_0g^2R\big),\\
P_\varepsilon &= \frac{5mR}{8\dot{\varphi}_*^2g}\Lambda_6, \qquad P_\theta = -\frac{5mR^2}{8\dot{\varphi}_*g}\Lambda_5,
\end{aligned} \tag{26}$$

where

$$\begin{aligned}
\Lambda_1 &= \sum_i \lambda_i, \qquad \Lambda_2 = \sum_{i<j} \lambda_i\lambda_j,\\
\Lambda_3 &= \sum_{i<j<k} \lambda_i\lambda_j\lambda_k, \qquad \Lambda_4 = \sum_{\substack{i<j\\<k<l}} \lambda_i\lambda_j\lambda_k\lambda_l,\\
\Lambda_5 &= \sum_{\substack{i<j<k\\<l<m}} \lambda_i\lambda_j\lambda_k\lambda_l\lambda_m, \quad \Lambda_6 = \lambda_1\lambda_2\lambda_3\lambda_4\lambda_5\lambda_6.
\end{aligned} \tag{27}$$

The controlled system can be stabilized by placing the characteristic roots λ_i to the left side of the complex plane, i.e., requiring, $\mathrm{Re}\lambda_i < 0$ for $i = 1, \dots, 6$.

The control gains (26) depend on the steady state pitch rate $\dot{\varphi}_*$, thus, the velocity $v_{\mathrm{P}',*} = R\dot{\varphi}_*$ of the unicycle has an essential role in control design. Two cases are considered in this study, one with subcritical speed

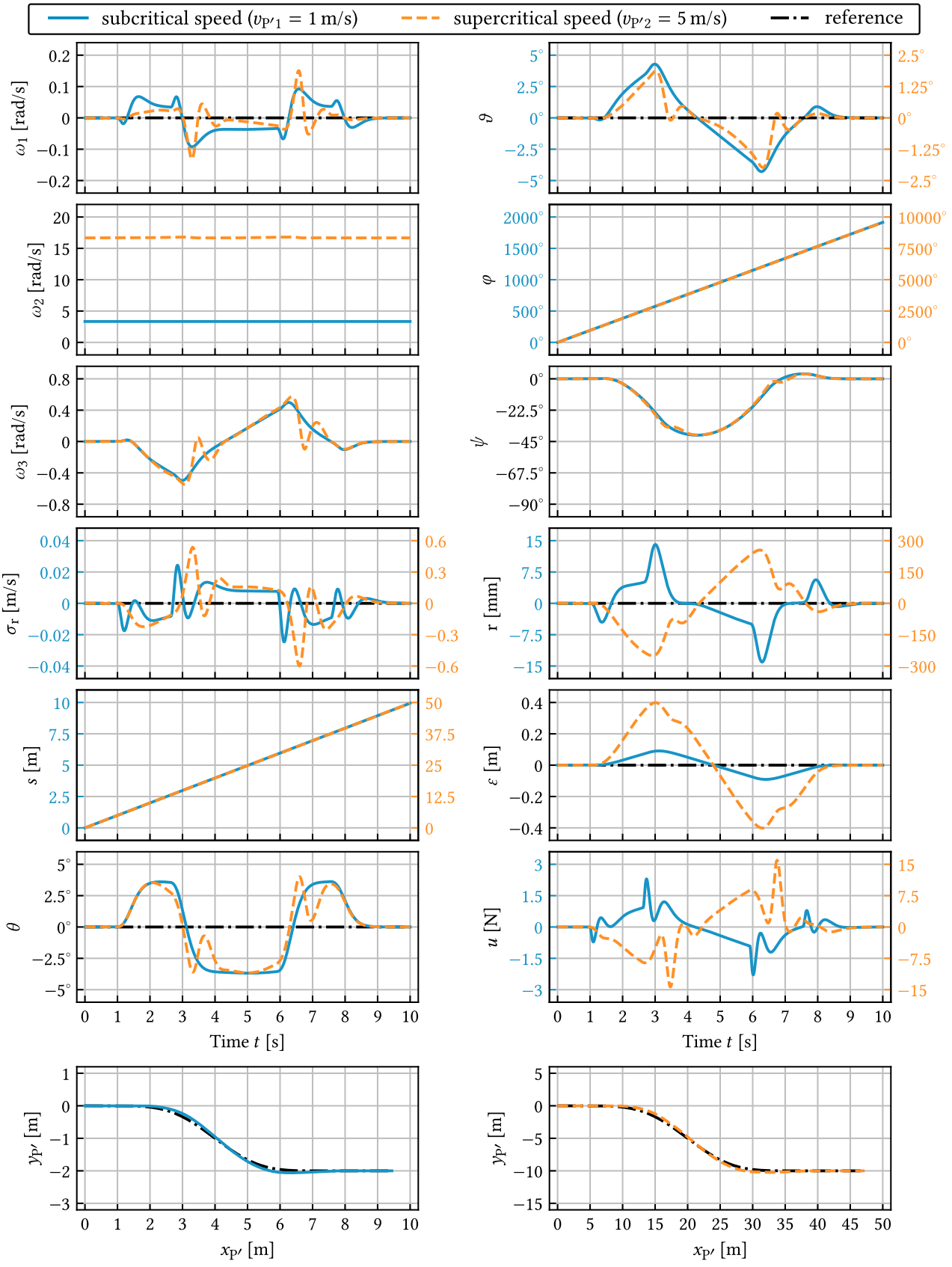

Fig. 3. Simulation results for lane change maneuver with subcritical and supercritical speeds.

Table 1. Physical parameters

Quantity	Value	
Disc mass m	10	kg
Disc radius R	0.3	m
Gravitational acceleration g	9.81	m/s^2
Point mass m_0	5	kg

Table 2. Control gains

Subcritical speed with $v_{\mathrm{P}',1} = 1\,\mathrm{m/s} < v_{\mathrm{P}',\mathrm{crit}}$		Supercritical speed with $v_{\mathrm{P}',2} = 5\,\mathrm{m/s} > v_{\mathrm{P}',\mathrm{crit}}$	
D_ϑ	−1407.64 Ns	D_ϑ	105.36 Ns
D_r	2116.86 Ns/m	D_r	99.52 Ns/m
P_ϑ	−8990.10 N	P_ϑ	723.17 N
P_r	11942.04 N/m	P_r	405.60 N/m
P_ε	4509.36 N/m	P_ε	180.37 N/m
P_θ	3382.02 N	P_θ	676.40 N

$v_{\mathrm{P}',1} = 1\,\mathrm{m/s} < v_{\mathrm{P}',\mathrm{crit}}$ and one case with supercritical speed $v_{\mathrm{P}',2} = 5\,\mathrm{m/s} > v_{\mathrm{P}',\mathrm{crit}}$, where the critical speed is

$$v_{\mathrm{P}',\mathrm{crit}} = R\dot{\varphi}_{\mathrm{crit}} \approx 1.21\,\mathrm{m/s}, \tag{28}$$

cf. (18). The numerical values of the physical parameters m, m_0, R and g can be found in Table 1. In both cases, the characteristic roots are chosen to be $\lambda_i = -8\,\mathrm{s}^{-1}$ for $i = 1, \ldots, 6$. The resulting control gains are given in Table 2.

The control performance is tested through simulations in which the control law (23) is applied to the nonlinear equations of motion (11). The initial condition for the subcritical case is $\omega_2(0) = v_{\mathrm{P}',1}/R$, while for the supercritical case, it is $\omega_2(0) = v_{\mathrm{P}',2}/R$, while the rest of the states were initialized as zeros. The simulation results are shown in Fig. 3; the autonomous unicycle successfully carries out the lane change maneuvers in both cases with sufficiently small error as shown by the panels for the lateral error ε and orientation error θ.

It is interesting to see that the point mass is located below the wheel for the lane change with subcritical speed as $\operatorname{sgn}\vartheta = \operatorname{sgn} r$, while the point mass is mostly above the wheel $\operatorname{sgn}\vartheta = -\operatorname{sgn} r$ during the maneuver with supercritical speed, see the corresponding panels in Fig. 3. We also highlight that only small control action is required: $u_{\max} \approx 2.5\,\mathrm{N}$ with $v_{\mathrm{P}',1}$ and $u_{\max} \approx 15\,\mathrm{N}$ with $v_{\mathrm{P}',2}$. We believe this is due to the fact that the controller utilizes the exact nonholonomic dynamics of the unicycle.

5. CONCLUSION

The spatial dynamics of autonomous unicycle has been considered and a control framework is proposed which enables the unicycle to execute maneuveres while following a planned path. By using the path-reference frame for control design, a single linear control law became capable to control the lateral motion and successfully carry out various maneuvers with the unicycle. The unicycle was able to follow the desired path with very small tracking errors while using small control forces. To further improve the path-following performance, a more sophisticated path-planning could be utilized via including the desired yaw rate through the desired tilt angle, which, for simplicity, was considered to be zero here.

REFERENCES

Antali, M. and Stépán, G. (2019). Nonsmooth analysis of three-dimensional slipping and rolling in the presence of dry friction. *Nonlinear Dynamics*, 97(3), 1799–1817. doi:10.1007/s11071-019-04913-x.

Appell, P. (1900). Sur une forme générale des équations de la dynamique (On a general form of the equations of dynamics). *Journal für die reine und angewandte Mathematik (Journal for Pure and Applied Mathematics)*, 121, 310–319. doi:10.1515/crll.1900.121.310.

Brown, H.B. and Xu, Y. (1996). A single-wheel, gyroscopically stabilized robot. In *Proceedings of IEEE international conference on robotics and automation*, volume 4, 3658–3663. IEEE. doi:10.1109/100.618022.

Cao, X., Bui, D.C., Takács, D., and Orosz, G. (2023). Autonomous unicycle: modeling, dynamics, and control. *Multibody System Dynamics*. doi:10.1007/s11044-023-09923-7.

Csernák, G. (2019). Analysis of pole acceleration in spatial motions by the generalization of pole changing velocity. *Acta Mechanica*, 230(7), 2607–2624. doi:10.1007/s00707-019-02408-9.

Geist, A.R., Fiene, J., Tashiro, N., Jia, Z., and Trimpe, S. (2022). The wheelbot: A jumping reaction wheel unicycle. *IEEE Robotics and Automation Letters*, 7(4), 9683–9690. doi:10.1109/LRA.2022.3192654.

Gim, K.G. and Kim, J. (2024). Ringbot: Monocycle robot with legs. *IEEE Transactions on Robotics*, 40, 1890–1905. doi:10.1109/TRO.2024.3362326.

Oh, S., Chen, Q., Tseng, H.E., Pandey, G., and Orosz, G. (2023). Sharable clothoid-based continuous motion planning for connected automated vehicles. *IEEE Transactions on Control Systems Technology*. URL `arxiv.org/abs/2312.10880`. (submitted).

Qin, W.B., Zhang, Y., Takács, D., Stépán, G., and Orosz, G. (2022). Nonholonomic dynamics and control of road vehicles: moving toward automation. *Nonlinear Dynamics*, 110(3), 1959–2004. doi:10.1007/s11071-022-07761-4.

Schoonwinkel, A. (1987). *Design and Test of a Computer Stabilized Unicycle*. Ph.D. thesis, Stanford University.

Suzuki, H., Moromugi, S., and Okura, T. (2014). Development of robotic unicycles. *Journal of Robotics and Mechatronics*, 26(5), 540–549. doi:10.20965/jrm.2014.p0540.

Vizi, M.B., Orosz, G., Takács, D., and Stépán, G. (2023). Steering control of an autonomous unicycle. *IEEE Transactions on Control Systems Technology*. URL `arxiv.org/abs/2307.08387`. (under review).

Vos, D.W. and von Flotow, A.H. (1990). Dynamics and nonlinear adaptive control of an autonomous unicycle: theory and experiment. In *29th IEEE Conference on Decision and Control*, volume 1, 182–187. doi:10.2514/6.1990-1241.

Zenkov, D., Bloch, A., and Marsden, J. (2002). The Lyapunov-Malkin theorem and stabilization of the unicycle with rider. *Systems & Control Letters*, 45, 293–300.